Model Based Development of Future Small Electric Vehicle by Modelica

Yutaka Hirano [1] Shintaro Inoue [1] Junya Ota [1]

[1]Toyota Motor Corporation, Japan, {yutaka_hirano, shintaro_inoue_aa, junya_ota}@mail.toyota.co.jp

Abstract

For future low carbon mobility society, new-type small electric vehicles (EVs) are developed actively in recent period. To reduce the energy consumption in various actual driving conditions, considering overall running resistance from tire characteristics, mechanical losses and electrical losses is necessary. In this paper, model-based development of system performance of a new EV is described. Full vehicle model considering both vehicle dynamics and energy consumption was developed using Modelica. Research for both structure and specification of components of the vehicle and also of the control were performed to find the solution to satisfy both energy consumption and vehicle dynamics by using the full vehicle model. Finally trade-off between vehicle stability and energy consumption and also between driver workload and energy consumption by using direct yaw moment control was indicated.

Keywords: Model Based System Development, Vehicle Dynamics, Energy Consumption, Electric Vehicle

1 Introduction

To satisfy needs for future low-carbon mobility society, development of many new small electric vehicles (EVs) is increasingly active in recent years. Those vehicles are often smaller and lighter than conventional vehicles and are often equipped with low RRC (Rolling Resistance Coefficients) tires for less energy consumption. On the other hand, low RRC tires tend to have less cornering performance than conventional tires in general. Because of light weight and low RRC tires, those vehicles become to have reduced dynamic stability against external disturbances such as side wind. To analyze and cope with all the problems about energy consumption and vehicle stability, a holistic approach of vehicle system design considering multi-physics of mechanics, electrics, aerodynamics, control and so on is necessary.

For this purpose, authors made an integrated model of the total vehicle system using acausal multi-domain physical modeling language Modelica (Hirano, 2014). By using Modelica, it is only necessary to define physical relationship written as equations in each component model and connect those component models as same as assembling the components to make the model of the whole system by hierarchical way. This feature of Modelica is very powerful for model-based system development because it enables to modify the whole vehicle model very easily by using the results of experiments and physical investigations of each component. It is just necessary to replace the existing equations of the component model to the modified ones and replace the component model to the revised one by object-oriented way.

In the previous paper (Hirano, 2014), authors showed the capability of new construction of the new EV using new type tire based on 'Large and Narrow concept' and torque vectoring differential gear. For the model based development of the new EV, various kind of running resistance, vehicle dynamic performance and proper design of electric regeneration system were studied.

In this paper, a multi-physics full vehicle model of the new EV is expanded to consider the detailed loss of motors and inverters. Also front and rear suspension model which has same 3D mechanical design as the real experimental vehicle was made and verified. By technical investigations using this full vehicle model, structure, specifications and control of the new EV system were researched about vehicle dynamics and energy consumption.

2 Characteristics of Target EV

Table 1. Specifications of new experimental EV

	New EV	Conventional car
Vehicle Weight	750 kg	1240 kg
Yaw Moment Inertia	869 kgm^2	2104 kgm^2
Wheelbase	2.6 m	2.6 m
Front : Rear Weight Distribution	0.48 : 0.52	0.62 : 0.38
Height of CG	0.38 m	0.55 m
Aerodynamic Drag × Frontal Area	0.392 m^2	0.644 m^2
Tire RRC	5×10^{-3}	8.8×10^{-3}
Tire Normalized CP	16.1	20.4

The proposed experimental EV has specifications as shown in Table 1. Compared with a conventional small-class passenger car, the new EV has characteristics of lighter vehicle weight, smaller yaw moment of inertia, lower height of the center of gravity

(CG) and lower RRC value of tires. Because of these characteristics, this new EV is expected to have better handling and lower energy consumption than conventional vehicles. On the other hand, because of lighter weight and lower value of tire normalized CP (Cornering Power), this new EV seems more sensitive against external disturbances such as crosswind and road irregularity than the conventional cars. To cope with this problem, direct yaw moment control (DYC) was applied by using a new integrated transaxle unit for rear axle which has a main electric motor and also torque-vectoring differential (TVD) gear unit with a control motor.

3 Full Vehicle Model

3.1 Structure of the Full-Vehicle Model

To consider total balance of energy consumption, handling, stability, ride comfort and NVH (noise, vibration, harshness) of the vehicle, a full vehicle model including mechanics, electronics, vehicle dynamics and control was developed based on commercially available Vehicle Dynamics Library (Modelon, 2014). The vehicle dynamics model was built as a full 3-dimentional (3D) multi-body-dynamics model of all of vehicle body, suspension, tires and power train. Aerodynamics was also considered in the vehicle dynamics model. Component models of control systems such as TVD gearbox, electric motor and inverter were newly developed and connected with the full vehicle model. The control logic for DYC was also implemented as a controller block model. Additionally, driving environment such as road shape, side wind and air parameters (density, temperature, etc.) can be defined as the environment model. Figure 1 shows the top level of model hierarchy of the full vehicle model.

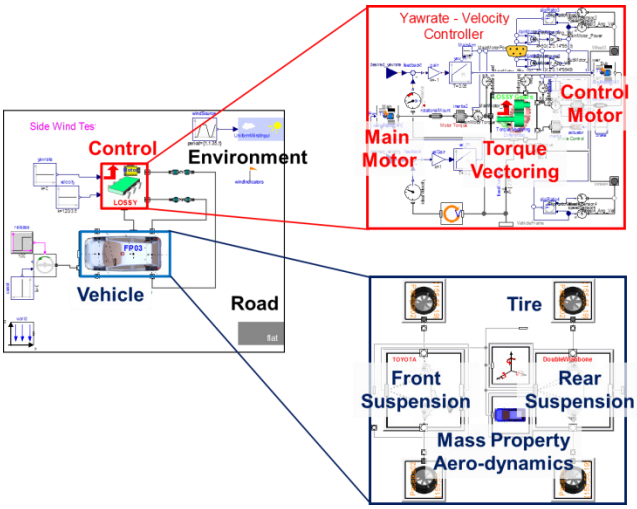

Figure 1. Top level structure of full vehicle mode

3.2 Mechanical Power by Driving Resistances

Power consumption of each system was calculated simultaneously to investigate the good balance of energy consumption and vehicle performances. At first, total mechanical power of driving resistances acting on the vehicle was calculated by following equations (Kobayashi et al., 2013).

Total driving resistance power:

$$P_v = P_{rr} + P_{ar} + P_{sy} + P_{sx} \quad (1)$$

Rolling resistance power:

$$P_{rr} = \mu_r Mg \times V \quad (2)$$

Aerodynamic resistance power:

$$P_{ar} = \rho A C_D V^2 / 2 \times V \quad (3)$$

Cornering drag resistance power:

$$P_{sy} = \left[\left(\frac{d_f}{C_{pf}} + \frac{d_r}{C_{pr}} \right) M A_y^2 / g \right] \times V \quad (4)$$

Longitudinal resistance power:

$$P_{sx} = (MA_x + Mg \sin\theta) \times V \quad (5)$$

Here

μ_r : tire rolling resistance coefficient (RRC) ,
g: acceleration of gravity [m/s^2],,
M: vehicle mass [kg],
V: vehicle speed [m/s],
ρ : air density [kg/m^3],
A: vehicle frontal area [m^2],
C_D : aerodynamic resistance coefficient,
d_f : front weight distribution ratio,
d_r : rear weight distribution ratio,
C_{pf} : front normalized cornering power [1/rad],
C_{pr} : rear normalized cornering power [1/rad],
C_p : average normalized cornering power [1/rad],
A_y : lateral acceleration [m/s^2],
A_x : longitudinal acceleration [m/s^2],
θ : road inclination [rad].

Total mechanical power of driving resistances can be calculated by equation (1) to equation (5) by using state variables of vehicle motion.

3.3 TVD Gear Train Model

For the TVD gear train, a driveline structure referencing the MUTE project of the Technische Universität München (TUM) (Höhn et al., 2013) was selected and the TVD model was constructed using commercially available Power Train Library (DLR, 2013) .

DOI 10.3384/ecp15118143

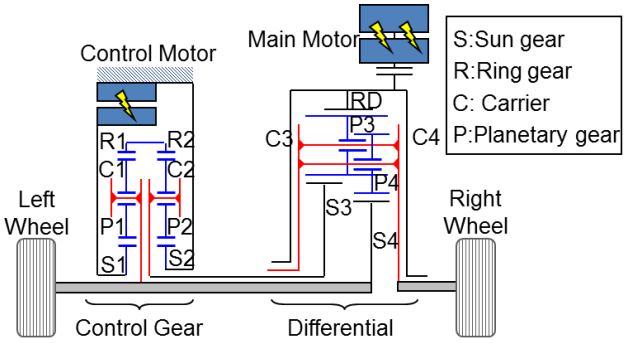

Figure 2. Torque vectoring differential (TVD) driveline

Figure 2 shows the configuration of the gear trains. This gear trains have a complex configuration constructed from several planetary gear sets. Torque from the main motor is distributed equally to the left and right wheel through the differential gear. Sun gear 3 is connected to carrier 2 in the control gear portion, and this configuration generates differences in torque between the left and right wheel by increasing or decreasing the torque distributed to the wheel on one side by torque input of the control motor. Specifications of the motors are shown in Table 2.

Table 2. Motor specification

	Main Motor	Control Motor
Max Torque	65 Nm	40 Nm
Max Speed	10,000 rpm	1,050 rpm
Max Power	15 kW	2 kW

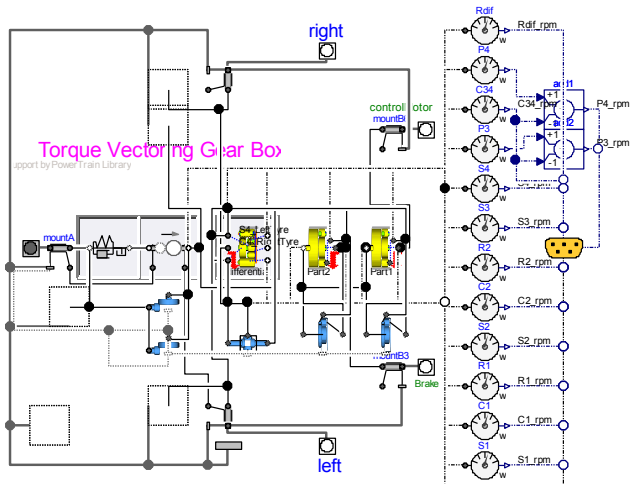

Figure 3. Modelica model of TVD gear train

Figure 3 shows a diagram of Modelica model of the torque vectoring gear train. The model is provided with elements that define the relational expression between the torque and speed of each gear engagement portion. Furthermore, these elements are capable of factoring in the overall gear torque loss by defining the torque loss for each element by following equations[7].

$$\Delta\tau = \begin{cases} (1-0.97)\tau_A & (\omega_{AB} > 0, \tau_A \geq 0) \\ (1-1/0.97)\tau_A & (\omega_{AB} > 0, \tau_A < 0) \\ (1-0.97)\tau_A & (\omega_{AB} < 0, \tau_A \geq 0) \\ (1-1/0.97)\tau_A & (\omega_{AB} < 0, \tau_A < 0) \end{cases} \quad (6)$$

where, τ_A is the sun gear torque and ω_{AB} is the difference in the speed of the sun gear and the carrier of the planetary gear.

Figure 4 shows a simulation result to investigate the torque distribution ability of the TVD. It became clear that this TVD unit has capability of distributing the driving torque between right and left wheels according to the input torque of the control motor and the torque distribution ratio can be bigger than ordinary LSD (limited slip differential) gear set if the mechanical strength is enough to cope with the maximum torque. The torque distribution ability is thus only limited by mechanical strength of the gear sets and the ability of the control motor.

Figure 5 shows an example of calculation result of each gear speed of the TVD. It was confirmed that this result coincide with the actual motion.

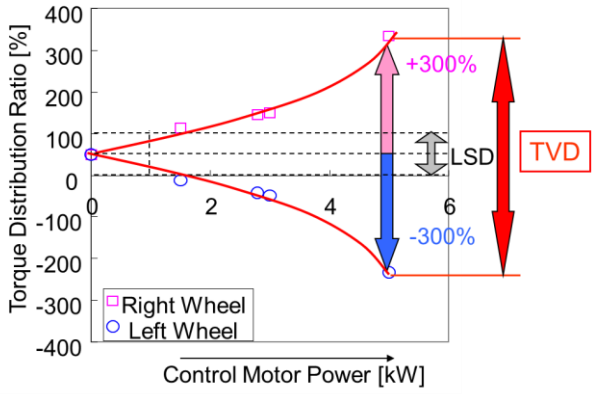

Figure 4. Torque distribution ability of TVD

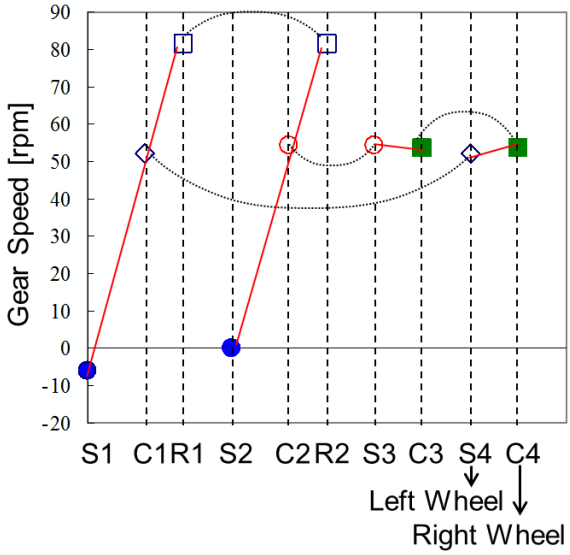

Figure 5. Example of TVD gear speed calculation

3.4 Electrical Model of Motor and Inverter

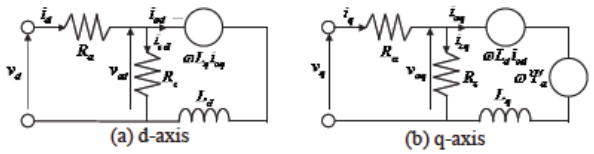

Figure 6. Equivalent circuits of each motor

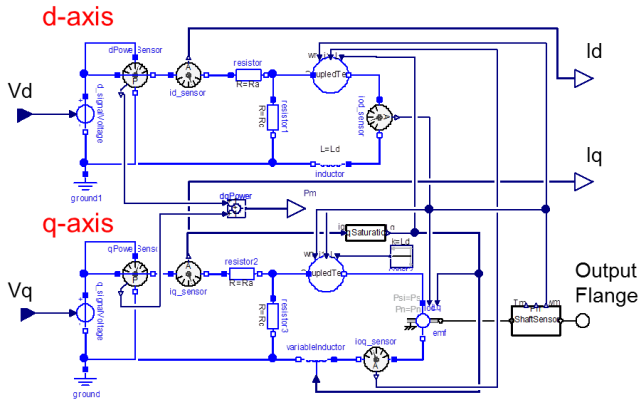

Figure 7. Electrical motor model by Modelica

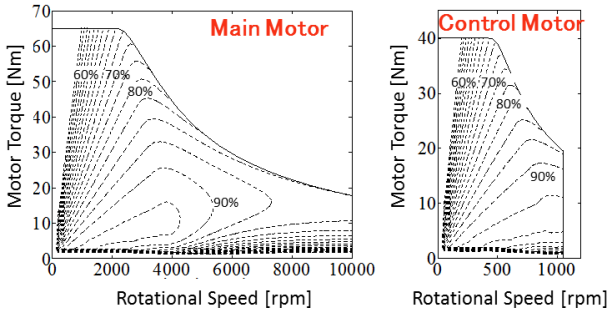

Figure 8. Motor characteristics

Both the main and control motors installed in the target EV are permanent magnet synchronous motors. The equivalent circuits of these motors can be expressed as shown in Figure 6 as d-axis and q-axis direct current (DC) circuits (Park, 1933). It is not necessary to describe the explicit equations here since modeling can be performed simply by laying out each device as shown in Figure 7 using freely available electric circuit library of Modelica Standard Libraries (MSL). Concurrently copper loss L_{Cu} and iron loss L_{Fe} of each motor are calculated using following equations (Inoue et al., 2014).

$$L_{Cu} = R_a I_a^{\,2} = R_a \left(i_d^{\,2} + i_q^{\,2} \right) \tag{7}$$

$$L_{Fe} = \frac{v_{od}^{\,2} + v_{oq}^{\,2}}{R_c} = \frac{\omega_e^{\,2} \left[\left(L_d i_{od} + \Psi_a \right)^2 + \left(L_q i_{oq} \right)^2 \right]}{R_c} \tag{8}$$

$$i_d = i_{od} + i_{cd}, \quad i_q = i_{oq} + i_{cq} \tag{9}$$

$$\begin{bmatrix} v_d \\ v_q \end{bmatrix} = R_a \begin{bmatrix} i_{od} \\ i_{oq} \end{bmatrix} + \left(1 + \frac{R_a}{R_c} \right) \begin{bmatrix} v_{od} \\ v_{oq} \end{bmatrix} + p \begin{bmatrix} L_d & 0 \\ 0 & L_q \end{bmatrix} \begin{bmatrix} i_{od} \\ i_{oq} \end{bmatrix} \tag{10}$$

$$\begin{bmatrix} v_{od} \\ v_{oq} \end{bmatrix} = \begin{bmatrix} 0 & -\omega_e L_q \\ \omega_e L_d & 0 \end{bmatrix} \begin{bmatrix} i_{od} \\ i_{oq} \end{bmatrix} + \begin{bmatrix} 0 \\ \omega_e \Psi_a \end{bmatrix} \tag{11}$$

where, v_d and v_q are the voltage of the d and q axis, respectively, i_d and i_q are the current of the d and q axis, respectively, ω_e is the electric angular velocity, R_a is the winding unbalance voltage attenuation, R_c is the equivalent iron loss resistance, L_d and L_q are the inductance of the d and q axis, respectively, and ψ_a is the inter-linkage magnetic flux. Also the motor characteristics of efficiency according to motor torque and rotational speed are considered as shown in Figure 8.

The inverter can be handled simply as a component that generates loss L_{inv} proportionally to the current vectors of the motors as follows.

$$L_{Inv} = \kappa I_a \tag{12}$$

3.5 Mechanical Model of Suspension and Body

3D multi-body dynamic system (MBS) models of suspension, steering and body were installed to calculate vehicle dynamics characteristics. Suspension model was constructed as an assembled model of each suspension linkage, joints and force elements such as spring, damper and bushing. Non-linear tire model based on 'Magic Formula' model (Pacejka02) was used to calculate combined lateral force and longitudinal force of each tire. Steering model considered the characteristics of viscous friction of steering gear box and steering shaft as well as steering shaft stiffness. By these detailed models, it became possible to analyze the effects of steering angle change and camber angle change caused by vehicle roll, side force and tire aligning torque.

Figure 9 shows a comparison of simulation results and experimental test results about camber angle change by wheel bump displacement and steering angle change by tire aligning moment. It was confirmed that the simulation results matched with the experimental results with good consistency.

Figure 10 shows an analysis result about the effect of suspension characteristics to cornering compliance coefficient normalized by the effect of tire slip angle change for one example of a front double wish-born suspension. It became clear that the effect of the tire aligning torque to tire toeing angle is relatively large than other design indexes.

Also 6 degree-of-freedom motion of the vehicle body was calculated by considering all the reaction forces and torques acting at suspension upper support and all of the connection portions of the linkages. Additionally 3D MBS model of TVD gear unit mounts was applied in the vehicle dynamics model. And rotational stiffness of the drive shafts was also considered. This feature enabled calculation of the body motion (mainly pitching motion) caused by the

DOI 10.3384/ecp15118143

reaction of driving torque and oscillation caused by resonance of tire rotational stiffness, drive shaft stiffness and differential gear mount stiffness.

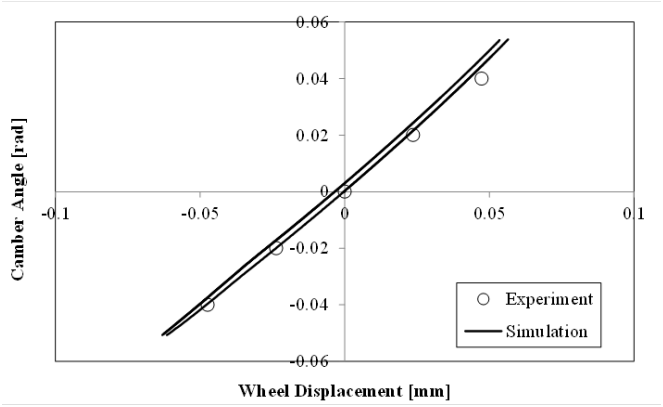

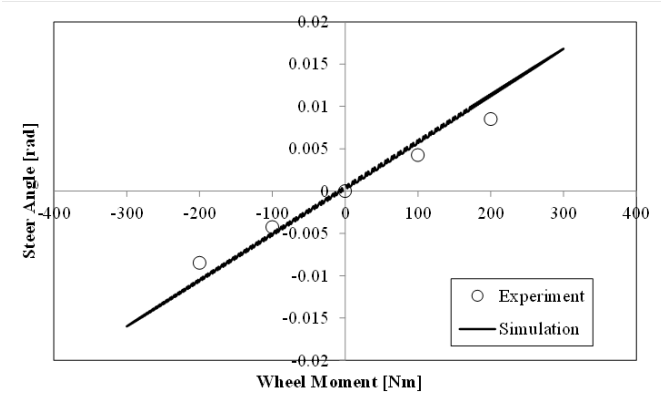

Figure 9. Example of suspension characteristics

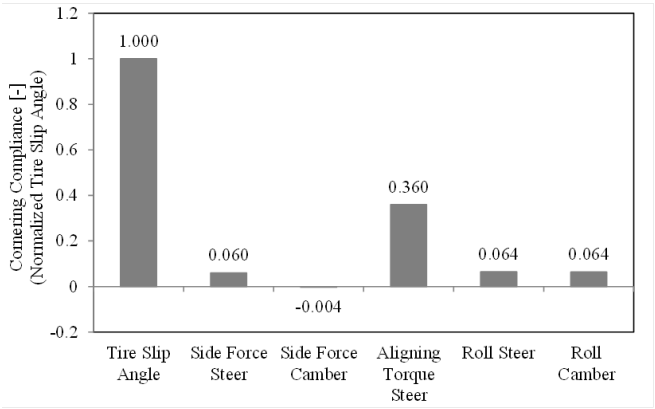

Figure 10. Effect of suspension characteristics to cornering compliance coefficient. (Normalized by the effect of tire slip angle.)

3.6 Model of DYC Controller

The control element generates the torque command values of the main motor and control motor. These command values are then input into the motor models. Two kinds of DYC controller were researched. Yaw rate feedback control to let the vehicle yaw rate follow the desired yaw rate for stabilizing crosswind disturbances comprises the control laws shown in Figure 11. Slip angle feedback controller shown in Figure 12 aims to let the vehicle slip angle to zero to stabilize the vehicle attitude while cornering and lane change.

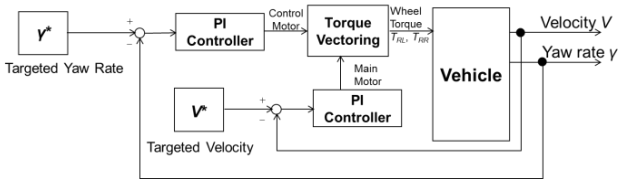

Figure 11. Yaw rate feedback controller of DYC

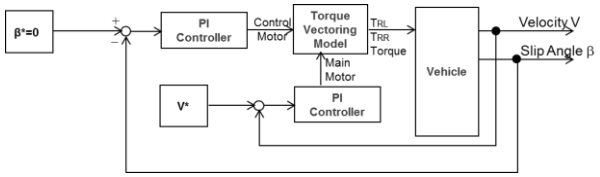

Figure 12. Slip angle feedback controller of DYC

In both controllers, the main motor performs feedback control by proportional and integral (PI) control of the vehicle speed because the vehicle speed is dominant for the total driving torque supplied by the main motor. The control motor performs feedback control by PI control of the yaw rate and vehicle slip angle respectively. As shown in Figure 4, control motor changes the distribution of left wheel torque T_{RL} and right wheel torque T_{RR}. Therefore the vehicle motion can be changed by yaw moment generated by the torque difference between left wheel and right wheel. In general, the vehicle motion can be estimated by single track model of vehicle dynamics described by equation (13) and (14).

$$\frac{d}{dt}\begin{bmatrix}\beta\\ \gamma\end{bmatrix}=\begin{bmatrix}-\frac{c_f+c_r}{MV} & -1-\frac{a_fc_f-a_rc_r}{MV^2}\\ -\frac{a_fc_f-a_rc_r}{I_z} & -\frac{a_f^2c_f+a_r^2c_r}{I_zV}\end{bmatrix}\begin{bmatrix}\beta\\ \gamma\end{bmatrix}+\begin{bmatrix}\frac{c_f}{MV} & \frac{c_r}{MV}\\ \frac{a_fc_f}{I_z} & -\frac{a_rc_r}{I_z}\end{bmatrix}\begin{bmatrix}\delta_f\\ \delta_r\end{bmatrix}+\begin{bmatrix}0\\ \frac{1}{I_z}\end{bmatrix}N \tag{13}$$

$$N = w(T_{RL} - T_{RR}) / r_t \tag{14}$$

Here,

- β : Vehicle slip angle [rad]
- γ : Yaw rate [rad/s]
- M : Vehicle mass [kg]
- V : Vehicle speed [m/s]
- I_z : Vehicle yaw moment of inertia [kgm^2]
- a_f : Length between front axle and CG [m]
- a_r : Length between rear axle and CG [m]
- l : Wheel base ($= a_f + a_r$) [m]
- c_f : Front tire cornering power [N/rad]
- c_r : Rear tire cornering power [N/rad]
- δ_f : Front tire steering angle [rad]

δ_r : Rear tire steering angle [rad]
N : Direct yaw moment [Nm]
r_t : Tire radius [m]
w : Tread [m]

3.7 Model of Energy Consumption by Electric Drives

Energy consumption in mechanical part (= gear train), electrical part (= motor, inverter) are calculated by using following equations.

$$P_e = P_m + L_{mj} + \sum_{j=1}^{2} L_{ej} \tag{15}$$

$$P_m = P_v + I_z\gamma = P_{rr} + P_{ar} + P_{sy} + P_{sx} + I_z\gamma \tag{16}$$

$$L_{mj} = 0.95 \times (T_M + T_C) \tag{17}$$

$$L_{ej} = L_{Cuj} + L_{Fej} + L_{Invj} \tag{18}$$

Here, P_e is the sum of the energy consumption, P_m is the total mechanical work using driving resistance power defined by equation (1), L_{mj} is the TVD mechanical loss, and L_{ej} is the electrical loss of motor and inverter. L_{Cuj} is copper loss, L_{Fej} is iron loss and L_{Invj} is switching loss of inverter respectively. Here, j=1 refers to the main motor and j=2 refers to the control motor. Since it is difficult to accurately calculate the TVD mechanical loss including all kinds of friction, the calculation assumes a constant overall efficiency of 95% of main motor torque T_M and control motor torque T_c.

Figure 13 shows the calculation results using the full-vehicle model in steady-state cornering with a turning radius of 60 m and a vehicle speed of 40 km/h. The calculated results using the full-vehicle model closely matched the theoretical results calculated based on Equations (15) and (16), thereby confirming the validity of this model. It is shown that electrical loss increases much when large DYC torque is applied.

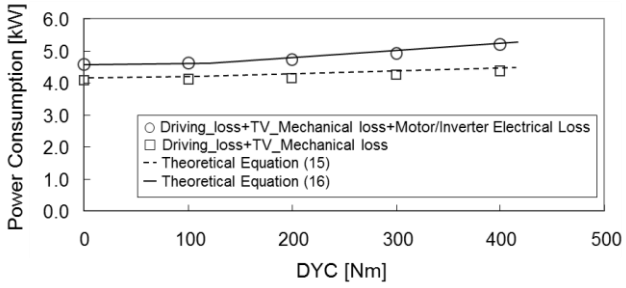

Figure 13. Comparison of energy consumption

4 Simulation Results

4.1 Steady State Cornering

The simulation of steady state cornering assumed running condition of a turning radius R of 135 m and a vehicle speed V of 60 km/h. Figure 14 shows the relationship between the vehicle slip angle and energy consumption in the β=0 control. Figure 15 shows the same relationship for the yaw rate feedback control. Here, the target yaw rate was calculated by following equation.

$$\gamma^* = K_{yaw\_gain} \times \frac{V}{R} \tag{19}$$

In the case of both controls, the turning resistance became lower as the slip angle and steering angle decreased. As a result, the power of the main motor decreased (point "i" in Figure 14 and Figure 15). In contrast, application of TVD generated mechanical loss, which resulted in an overall increase in energy consumption due to the energy consumption of the control motor (point "ii" in Figure 14 and Figure 15). Furthermore, the TVD mechanical loss was lower than the electrical loss. This result indicates that, in this configuration, a reduction in motor/inverter electrical loss is extremely important for reducing energy consumption. Finally, further examination of the β=0 control in Figure 14 shows that a very slight vehicle slip angle remains when the control is applied (point "iii" in Figure 14). Focusing on the TVD control motor torque shows that, in an ideal condition without TVD or motor/inverter loss (Figure 16), the vehicle slip angle is zero because the power of the control motor does not exceed the maximum possible output torque of 40 Nm. However, after factoring in each type of loss, the control motor power becomes saturated (point "iv" in Figure 16). In this way, integrating different physical models into a single model enables quantitative studies of the effects of each type of loss on vehicle dynamics and control.

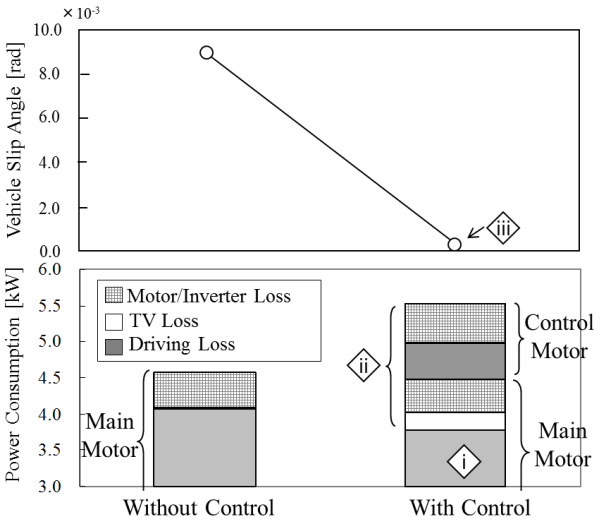

Figure 14. Energy consumption with β=0 control

DOI 10.3384/ecp15118143

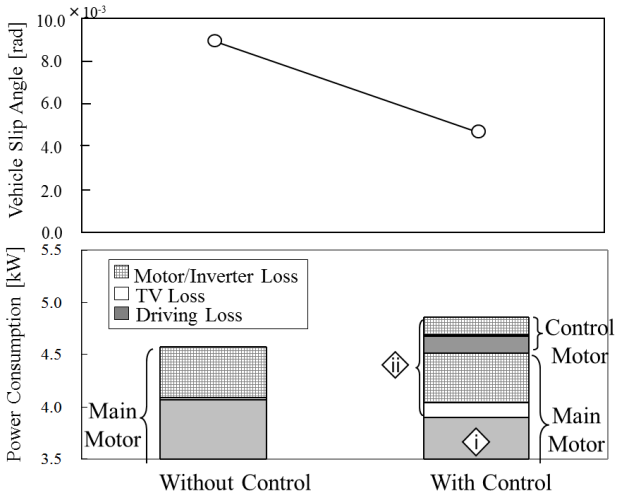

Figure 15. Energy consumption with yaw rate feedback Control

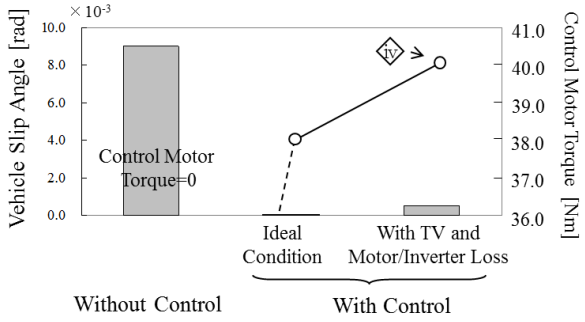

Figure 16. Relationship between vehicle slip angle and control motor torque with β=0 control

4.2 Winding Road Driving

Actual driving conditions generally feature many turns and the proposed EV is also likely to be driven while utilizing controls to actively enhance dynamic performance. Therefore, to simply evaluate performance under real-world driving conditions, a study was performed on winding roads to simulate actual continuous steady-state cornering. The study simulated an actual 8.1 km winding road course, which combines straight sections and gradients.

First, the course was constructed using the commercially available CarMaker software. Driving behavior was predicted using a driver model of CarMaker assuming a constant speed of 60 km/h. Developed Modelica model of TVD was connected with CarMaker using FMI (Functional Mockup Interface). Only vehicle speed was set in the driver model and lateral acceleration was calculated during the simulation. By using CarMaker as a virtual driving test platform, it became possible to combine the good realistic driver model of CarMaker and the detailed drive train model made by using Modelica.

Finally, the energy consumption and steering wheel angle by the driver model were predicted using the time-series data for lateral acceleration in Figure 17.

Figure 18 shows the time-series data for the total energy consumption and steering wheel angle with a yaw gain ratio of 1.5. (Abbreviation of 'W/O Control' means 'Without Control'.) Although yaw gain control causes an increase in total energy consumption, the steering wheel angle decreases. These prediction results facilitate the identification of the optimum control gain with respect to a set system configuration, assuming real-world driving conditions.

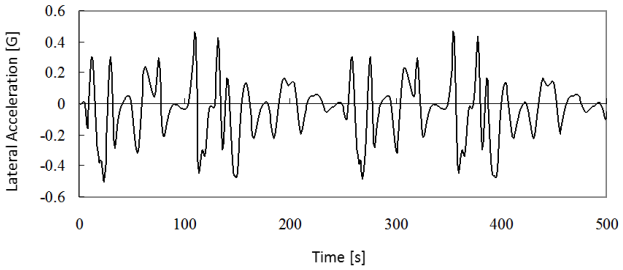

Figure 17. Time-series data for lateral acceleration

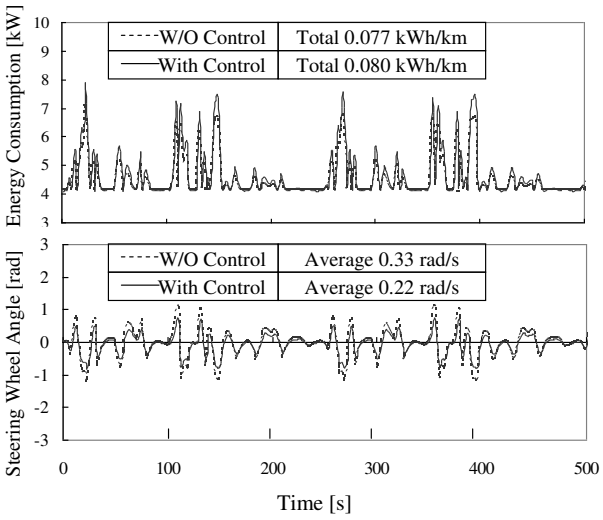

Figure 18. Time-series data (upper: energy consumption, lower: steering wheel angle)

5 Conclusions

This paper described the development of a full-vehicle model to quantitatively evaluate the relationship between vehicle dynamics with DYC input and energy consumption for a small EV. The following conclusions were obtained.

(i) TVD drivelines with several planetary gear sets and motor/inverters with multiple electrical elements can be constructed simply in one model using Modelica.

(ii) The model was able to quantitatively identify the breakdown of energy consumption increases and decreases for achieving the target vehicle dynamics. In addition, it was found that reducing motor loss makes a larger

contribution to lower energy consumption than reducing TVD mechanical loss.

(iii) The real-world energy consumption and driver's workload (steering wheel angle) through DYC was predicted on a simulated course based on actual winding roads.

For future works, it is planned to consider the effect of drive shaft stiffness for TVD control. Also controlling tire slip by motor torque as well as maximizing regeneration by breaking is essential to expand the capability of electric control of optimal tire slip control. This work will also be useful to design a proper system configuration of mechanical break and electric break and also designing proper torque blending control.

References

DLR, PowerTrain Library Users Guide (Version 2.1.0), 2013

Y. Hirano, S. Inoue and J. Ota, Model-based Development of Future Small EVs using Modelica, *Proceedings of Modelica Conference 2014*, 2014.

B. Höhn et al., Torque Vectoring Driveline for Electric Vehicle, *Proceedings of the FISITA 2012 World Automotive Congress*, Vol. 191, pp. 585-593, 2013.

S. Inoue, J. Ota, Y. Hirano, T. Kobayashi, A. Kawaguchi and H. Sugiura, Study on Full-Vehicle Model Integrating Vehicle Dynamics and Energy Consumption, *Proceeding of 12th International Symposium on Advanced Vehicle Control (AVEC'14)*, 20149329, 2014.

T. Kobayashi, E. Katsuyama, G. Sugiura, E. Ono, M. Yamamoto, A research about driving force distribution control and energy consumption while cornering, *Proceeding of 2013 JSAE Annual Congress (Spring)*, 352-20135393, 2013 (in Japanese).

Modelon, A.B., Vehicle Dynamics library Users Guide (Version 1.8), 2014.

R.H.Park, Two-reaction Theory of Synchronous Machines: Part II, *AIEE Trans.*, Vol.52, pp.352-355, 1933.

C. Pelchen et al., Modeling and Simulating the Efficiency of Gearboxes and of Planetary Gearboxes, *Proceedings of 2nd International Modelica Conference*, pp. 257-266, 2002.

 DOI 10.3384/ecp15118143